AIAA SciTech Forum
January 3-7, 2022, San Diego, CA & Virtual
AIAA SCITECH 2022 Forum

10.2514/6.2022-1446

Soot prediction in a Model Aero-Engine Combustor using a Quadrature-based method of moments

Ömer Hakkı Çokuslu* and Christian Hasse†
TU Darmstadt, Otto-Berndt-Str. 2, 64289 Darmstadt, Germany

Klaus-Peter Geigle‡
German Aerospace Center (DLR), Pfaffenwaldring 38-40, 70569 Stuttgart, Germany.

Federica Ferraro§
TU Darmstadt, Otto-Berndt-Str. 2, 64289 Darmstadt, Germany

Numerical simulations of aero-engine combustors are extremely challenging due to the complex multiscale and multiphysics phenomena involved. Currently, reliable modeling and prediction of soot particle formation produced during incomplete hydrocarbon combustion is one of the major issues in combustion research. The next generation of gas turbines for more sustainable aircraft engines must meet strict limitations for soot particle mass and size distribution. Therefore, a comprehensive understanding of the processes leading to soot particle formation and its precise prediction in practical combustion systems is crucial. In this work, a recently developed detailed soot model, the Split-based Extended Quadrature Method of Moments (S-EQMOM), is applied to simulate a model aero-engine combustor, experimentally investigated by the German Aerospace Center (DLR). In previous studies, the S-EQMOM demonstrated good prediction capability in predicting soot particle oxidation, important to account for the reduction of soot particles. Here, the model is evaluated at elevated pressure conditions. Large eddy simulations are performed using flamelet-based tabulated chemistry with artificially thickened flame (ATF) approach coupled with the S-EQMOM. The simulation results are analyzed for both the gas phase and soot solid phase and compared with the experimental data. Velocity and temperature fields are well predicted. Soot formation is underestimated by the simulation, but qualitatively in good agreement with the experimental data.

I. Introduction

The next-generation of aircraft combustors needs to be designed to minimize pollutant emissions while improving thermal efficiency. Especially, soot emissions, generated by incomplete combustion of hydrocarbon fuels, are particularly harmful to human health and have detrimental effects on the global climate. Therefore, recent emission control regulations introduced limits for the mass and number of soot particles emitted by internal combustion engines and gas turbines [1].

Soot emissions originate from complex multiscale interactions between turbulence, chemical reactions, and particle evolution, which take place over a large range of time and space scales. Significant research efforts have been devoted to understand pollutant formation processes and to identify possible strategies to reduce them. However, modeling particle formation and growth pathways in turbulent reacting flows still represent a challenge in combustion research.

Recently, Large-Eddy Simulations (LES) have been employed to simulate laboratory-scale turbulent sooting flames, e.g., [2–6], and model aero-engine combustion chambers [7–11] exploring different combustion models, turbulence-chemistry interaction closure and soot models. While turbulent reacting flows can be predicted with a high level of accuracy, uncertainties are found in the prediction of soot chemistry and particle dynamics and their interaction with turbulence [12].

*PhD Student, Institute for Simulation of Reactive Thermo-Fluid Systems.
†Professor, Institute for Simulation of Reactive Thermo-Fluid Systems.
‡Senior Research Scientist, DLR-VT Institute of Combustion Technology.
§Postdoctoral researcher, Institute for Simulation of Reactive Thermo-Fluid Systems.

Among several detailed soot models, the extended Quadrature Method of Moments (EQMOM) approach [13] and the Split-based Extended Quadrature Method of Moments (S-EQMOM) [14] have shown to be suitable for soot prediction, since they provide a continuous reconstruction of the particle Number Density Function (NDF), particularly important when soot particle oxidation needs to be considered. Indeed, this information can be used to model the complete oxidation of the smallest particles consistently as it has been shown in [14]. In the S-EQMOM the NDF is approximated by the sum of sub-NDFs of a known shape, e.g. gamma or lognormal distributions, interacting through the coagulation term. The S-EQMOM proposes an alternative formulation of the EQMOM approach from Yuan et al. [13], in which the NDF is approximated by a weighted sum of kernel density functions. In the S-EQMOM the moments of sub-NDFs are considered instead of the moments of the entire NDF. The main advantage of the S-EQMOM over the EQMOM is that the inversion procedure yields a system of equations that is solved analytically and has a unique solution [14], while, in the EQMOM, an iterative and non-unique procedure [13, 15, 16] is applied to invert the moments, from low and high order moments of the entire NDF. Therefore, the S-EQMOM formulation greatly improves the stability of the inversion algorithm, allowing a computationally efficient and robust local reconstruction of the soot particle NDF, which is crucial when the model is employed in the LES context. The S-EQMOM does not only provide the soot volume fraction but is also able to predict the local particle size distribution (PSD), not available in classical methods of moments.

The recently developed S-EQMOM has been applied in laminar premixed flames at highly oxidating conditions [14] and in a turbulent jet flame at atmospheric pressure [6]. In this work the S-EQMOM is employed to simulate a model aero-engine combustor at increased pressure conditions designed and experimentally characterized at the German Aerospace Center (DLR) [17–19]. Here LES are performed using tabulated chemistry based on the flamelet-progress variable approach for the combustion closure and the artificially thickened flame (ATF) model to account for the turbulence-chemistry interaction (TCI) combined with the S-EQMOM.

The DLR model combustor features flow and flame characteristics of a Rich-Burn/Quick-Quench/Lean-Burn (RQL) type aero-engine combustor. Primary air is supplied into the combustion chamber through a central and annular nozzle. The airflows are separated and pass radial swirlers forming a recirculation zone with a turbulent rich primary combustion zone. Gaseous fuel (C_2H_4) is injected in between both airflows. Secondary air is injected into the chamber through four holes located in the corners of the combustion chamber at an axial position of 80 mm, leading to a RQL-type soot oxidation region. The measurements by Geigle et al. [17–20] provide velocity field information in both cold and reacting conditions as well as temperature and soot volume fraction data at various operating conditions, i.e. different pressure levels up to 5 bar, equivalence ratio, and with and without oxidation air.

Recent works investigated the DLR burner with various modeling approaches. Eberle et al. [8] analyzed the DLR burner using unsteady Reynolds Averaged Navier-Stokes simulations (RANS) with finite-rate chemistry. The evolution of the Polycyclic Aromatic Hydrocarbons (PAHs) were described with a sectional approach and the soot particle evolution with transport equations for the soot mass fraction and the soot particle number density. Excellent agreement was obtained for velocity and temperature fields compared to the experiments and a reasonable agreement was obtained for the soot volume fraction. LES using finite-rate chemistry model combined with assumed probability density function for the turbulence-chemistry interaction were performed by Grader et al. [11]. PAHs and soot were modeled using a sectional approach. A good to excellent agreement was found in velocity, temperature and OH distributions. The qualitative distributions of soot volume fraction was also captured satisfactorily. Dupoirieux et al. [21] and Franzelli et al. [7] performed LES using different combustion models, tabulated chemistry [7, 21] and reduced chemistry [7], combined with the ATF approach with a two equations soot model. Simulations of the 3 bar case with secondary air showed a satisfactory prediction of the temperature and soot field. Wick et al. [10] conducted LES using a Radiation Flamelet/Progress Variable approach to model combustion and Hybrid Method of Moments (HMOM) for the soot particle evolution. A transport equation for C_2H_2 mass fraction is solved to account for the consumption of the species involved in the soot surface reactions. The soot field was over-predicted by the model but qualitatively in reasonable agreement with the experimental data [10]. In [22] simulations of the 3 bar and the 5 bar cases with secondary oxidation air were conducted using LES and the dynamic thickened flame model. Two combustion closure approaches, the Analytically Reduced Chemistry (ARC) and tabulated chemistry, were compared. While the overall flame features were predicted similarly well with both chemistry models, the analytically reduced chemistry could predict the flame structure and soot concentration more accurately with an increase in CPU time. Chong et al. [9] examined the effect of pressure and secondary oxidation air on soot formation using LES. The combustion has been described by a set of tabulated flamelets including heat loss through radiation. The walls are considered adiabatic. 3 bar and 5 bar cases were examined with and without oxidation air. The simulations predicted gas-phase statistics accurately. Soot formation was captured well, although the soot peaks in the inner recirculation zone were not predicted. The reduction in soot

concentration in the presence of side jets was observed, while acetylene-based growth was found to be the dominant process in the soot mass addition. In Chong et al. [23], different models for chemical kinetics and description of soot population are compared to each other. The semi-empirical soot model [24], the detailed Hybrid Method of Moments (HMOM) [25] and the conditional Quadrature Method of Moments (CQMOM) [26] are applied to simulate the 3 bar case without oxidation air. This comparison revealed the soot sensitivity to the choice of the model, due to differences in the growth pathways and their dependence on mixture fraction. HMOM and CQMOM, both PAH-based models, tend to generate soot in the shear layers, where rapid changes in strain rate lead to intermittency in soot inceptions [23], while the semi-empirical model, which is an acetylene-based model, over-predicts significantly the soot volume fraction in the inner recirculation zone. Gallen et al. [27] used a Lagrangian approach to track soot particles, which is applied to LES calculating the flow field parameters. In comparison with the Eulerian approach, the Lagrangian model produces similar results for soot in magnitude and distribution while maintaining a similar computation time. In [28] LES of the DLR burner were conducted using the optically thin model (OTM) for radiation modeling and imposing temperatures on the wall measured by Nau et al. [29]. The use of the OTM reduces the axial temperature by more than 100 K. It showed that the radiation has a strong impact on the temperature as well as on flame shape and flame stabilization. In [30] the soot model performance based on parametric studies is evaluated and the contribution of the soot intermittency model to the prediction of soot production is investigated. The focus has been put on the description of the soot surface growth mechanism. A modification of the well-known H-abstraction-C_2H_2-addition (HACA) mechanism has been proposed and an improvement in predicting soot volume fraction was observed.

In this context, the objective of this work is to assess the performance of the recently developed S-EQMOM soot model on the DLR model combustor, which is a well-established benchmark case for soot model development.

The paper is structured as follows: first, the numerical modeling approach is described along with the investigated configuration and the numerical setup; subsequently, simulation results of the flow field and the particulate phase are discussed. In conclusion, the numerical approach for soot modeling is evaluated.

II. Numerical modeling

A. Combustion Model

In the LES, Favre-filtered Navier-Stokes equations are solved to describe the flow field evolution. The turbulence closure is achieved with the sigma model [31]. Chemical reactions are accounted for using a tabulated combustion model based on the flamelet-progress variable approach [32, 33]. The flamelet database is generated solving a series of one-dimensional adiabatic freely propagating premixed flames [34]. Different levels of enthalpy have been included following the procedure described in [35] to account for the heat losses towards the walls. The flamelets are then tabulated and stored in a look-up library, which is accessed during runtime to retrieve thermochemical quantities needed for the solution of the momentum and scalar equations, similar to the approach in [36]. The thermochemical state is parametrized by the mixture fraction Z, the progress variable Y_C and the enthalpy h resulting in the description $\phi = \phi(Z, Y_C, h)$. Here, the progress variable is defined as $Y_C = Y_{CO_2} + Y_{CO} + Y_{H_2O} + Y_{H_2}$. The one-dimensional flames are calculated with the kinetic mechanism from Blanquart and Pitsch [37] and Narayanaswamy et al. [38] assuming unity Lewis number. The mechanism contains detailed PAH chemistry up to C_{16} and C_{18} species (pyrene, etc.) and has been used in previous works on the same configuration e.g., [9, 23].

The turbulence-chemistry interaction is accounted for with the artificially thickened flame (ATF) approach [39]. The efficiency function E is modeled with the approach by [40] and the required model constant is set to $\beta = 0.5$, while the flame sensor is defined according to the definition by Popp et al. [41].

B. Soot Model

In this work two sub-NDFs with gamma-distribution are considered for describing soot formation with the S-EQMOM [14], which consists of solving six additional transport equations for the moments, i.e. the three low-order moments of each sub-NDFs. The transport equation for the moments reads

$$\frac{\partial \bar{m}_k(x_i,t)}{\partial t} + \frac{\partial \tilde{u}_i^* \bar{m}_k(x_i,t)}{\partial x_i} = \frac{\partial}{\partial x_i}\left(D_T \frac{\partial \bar{m}_k(x_i,t)}{\partial x_i}\right) + \dot{\bar{m}}_k(x_i,t). \tag{1}$$

Here u_i^* is the total velocity including the thermophoresis effect. D_T represents the turbulent diffusivity, determined as ν_T / Sc_T with ν_T the eddy viscosity and Sc_T the turbulent Schmidt number set equal to 0.7. The source terms of

the moment equations include particle nucleation from two PAH molecules, surface growth by condensation of PAH molecules on soot particles, HACA mechanism, coagulation and particle oxidation by reactions with O_2 and OH. The source term closure is obtained with the S-EQMOM algorithm described in detail in [14]. To describe the slow PAH chemistry and the mass transfer from gas to solid phase due to nucleation of soot particles, a filtered transport equation for the PAH mass fraction is solved in the LES, following [2]

$$\frac{\partial \bar{\rho}\tilde{Y}_{PAH}}{\partial t} + \frac{\partial \bar{\rho}\tilde{u}_i\tilde{Y}_{PAH}}{\partial x_i} = \frac{\partial}{\partial x_i}\left(\bar{\rho}\left(\tilde{D} + D_T\right)\frac{\partial \tilde{Y}_{PAH}}{\partial x_i}\right) + \bar{\omega}_{PAH}. \tag{2}$$

Here $\tilde{Y}_{PAH}$ is the sum of A4 (pyrene) and A4R5 (cyclopenta[cd]pyrene) considered as PAH soot precursors. According to [2, 33] the filtered source term $\bar{\omega}_{PAH}$ is decomposed in three components: a chemical production term $\bar{\omega}^{+}_{PAH}$, which is independent of the species concentration, a chemical consumption term $\bar{\omega}^{-}_{PAH}$, which is linear with the species concentration, and a consumption term representing the mass transfer rate from gas-phase to soot $\bar{\omega}_{nuc}$, which is quadratic with the species concentration. The filtered source term is then decomposed as

$$\bar{\omega}_{PAH} = \bar{\omega}^{+T}_{PAH} + \bar{\omega}^{T}_{PAH}\left(\frac{\tilde{Y}_{PAH}}{\tilde{Y}^{T}_{PAH}}\right) + \bar{\omega}^{T}_{nuc}\left(\frac{\tilde{Y}_{PAH}}{\tilde{Y}^{T}_{PAH}}\right)^2, \tag{3}$$

where the superscript T indicates the value obtained from the flamelet table. Numerical simulations are performed with an in-house solver developed into the OpenFOAM framework [6, 36, 42].

III. Numerical setup

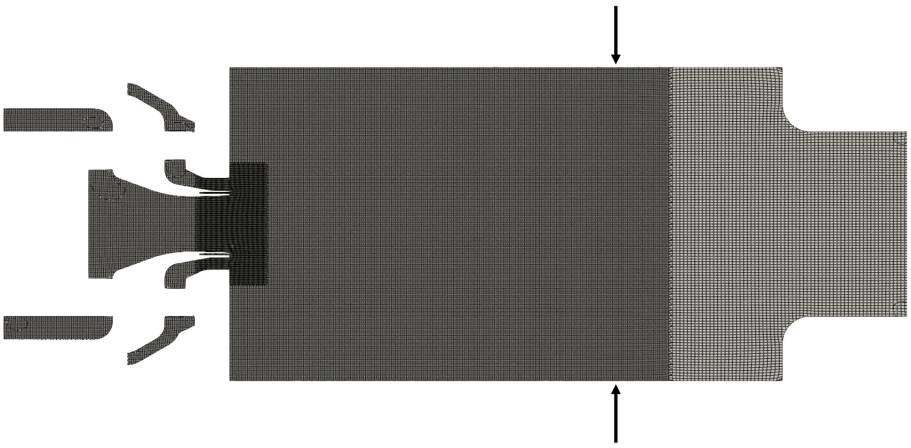

Fig. 1 Numerical grid of the DLR combustion chamber. A middle plane through the chamber is shown. Arrows indicate the position of secondary air injection.

The burner and operating points are described in detail in [17–20]. In this work, the 3 bar operating point with secondary air injection is investigated [20]. Air at ambient temperature $T = 298$ K is injected primarily into the combustor through a dual swirl system. The inner central nozzle of the dual swirl system supplies 30% of the primary air. The remaining 70% of the swirling primary air is introduced through the concentric outer annular nozzle. Ethylene is used as a fuel and is injected through 60 tiny quadratic channels located between the two swirlers forming a concentric ring. Fuel and primary airflow rates result in an equivalence ratio of $\phi_{primary} = 1.2$. The secondary air flow rate accounts for 40% of the primary air flow rate, such that a global equivalence ratio of $\phi_{global} = 0.86$ is reached.

The computational grid is presented in Fig. 1. It is hexa-dominant and consists of 15.6 million cells. To accurately predict the fuel-air mixing and consequently the reacting flow features into the combustion chamber the grid is refined locally at the swirler exit regions and up to the secondary air injection. The smallest cell size (0.1 mm) is located in the fuel injector (width 0.4 mm). Mass flow rates given in [17–20] are prescribed at the fuel injector and air swirler inlets. No-slip boundary conditions are used at the combustor walls. For the pressure a Dirichlet boundary condition is applied at the outlet. At the lateral combustor walls the temperature distribution measured by Nau et al. [29] is applied

as the temperature boundary condition. At the bottom walls, a temperature equal to 650 K has been considered with experimental uncertainty of about +/- 100 K as suggested in [18].

IV. Results

The reacting gas phase is first analyzed in terms of the velocity field. Figure 2 illustrates the time-averaged axial velocity along the centerline of the combustor. Two different PIV data evaluation techniques were used to describe the velocity field, namely the Field of View method (PIV-FoV) and the Sum of Correlation method (PIV-SoC) [17]. According to [17], the field of view (PIV-FoV) profiles are more reliable but do not cover the entire combustor. The PIV-SoC provides only time-averaged velocities, while instantaneous and RMS velocities can be obtained by PIV-FoV (field of view) as presented in [17]. Therefore both sets of data are plotted in Fig. 2. The simulation results slightly overpredict the experimental data in the inner recirculation zone, identified by the negative velocity, while comparing very well downstream of the secondary air injection.

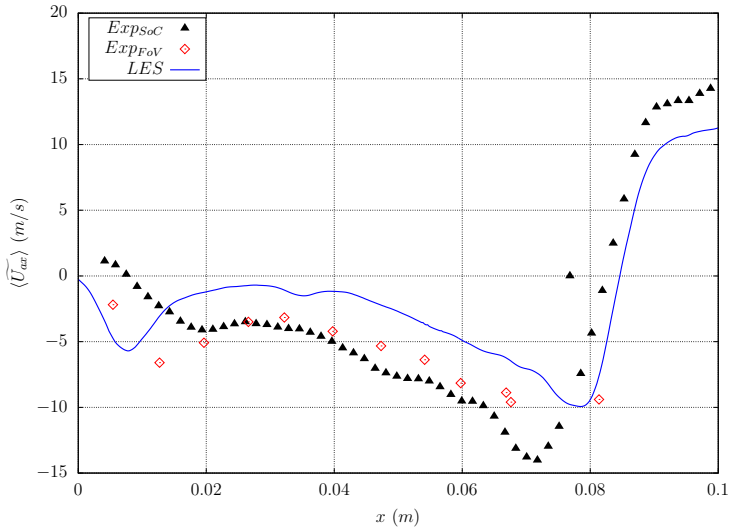

Fig. 2 Time-averaged axial velocity component along the centerline of the combustor. Experimental data are from [17].

Time-averaged axial, radial, and tangential velocity profiles are compared with the experimental data in Fig. 3 at three axial locations. At $x = 0.012$ m, velocity peaks characterize the flow field between the inner and outer shear layers. Negative axial velocities close to the centerline indicate that the inner recirculation zone extends into the vicinity of the primary swirlers. A good agreement is observed between simulation and FoV-data for all velocity components. Similarly, a good prediction is observed at $x = 0.015$ m. At $x = 0.065$ m, the velocity distribution becomes more homogeneous. It is to be noted that the high soot luminosity complicates the evaluation of experimental data, which leads to deviations between PIV-SoC and PIV-FoV data, especially at $x = 0.012$ m in the vicinity of the lateral walls. The agreement level of radial and tangential velocities with the measurements shows that the simulations are very good at capturing the flow structure, including the details of the recirculation zone.

The simulated time-averaged axial velocity and temperature distribution in the chamber can be seen in Fig. 4. The white isoline indicative of zero axial velocity illustrates the large inner recirculation zone (IRZ) and small outer recirculation zones. At $x = 0.08$ m the secondary air is injected contributing to the upstream flow in the inner recirculation zone, which extends up to the primary swirler. The hot gases are mixed with the injected air and transported upstream into the primary combustion zone. The temperature field is nearly uniform in the near-nozzle region with a V-shaped mixing characteristics. Downstream the temperature in the IRZ decreases as a result of interaction of the secondary air injection with the hot combustion gases generated from the primary injection. Moreover, as shown in Fig. 4, the injected secondary air leads to secondary oxidation (and in consequence heat release) downstream of the primary combustion zone in the vicinity of lateral walls.

Figure 5 shows the comparison of measured and simulated time-averaged temperature profiles on the centerline of the combustor. The time-averaged temperature evolution is correctly captured by the simulation taking into account the

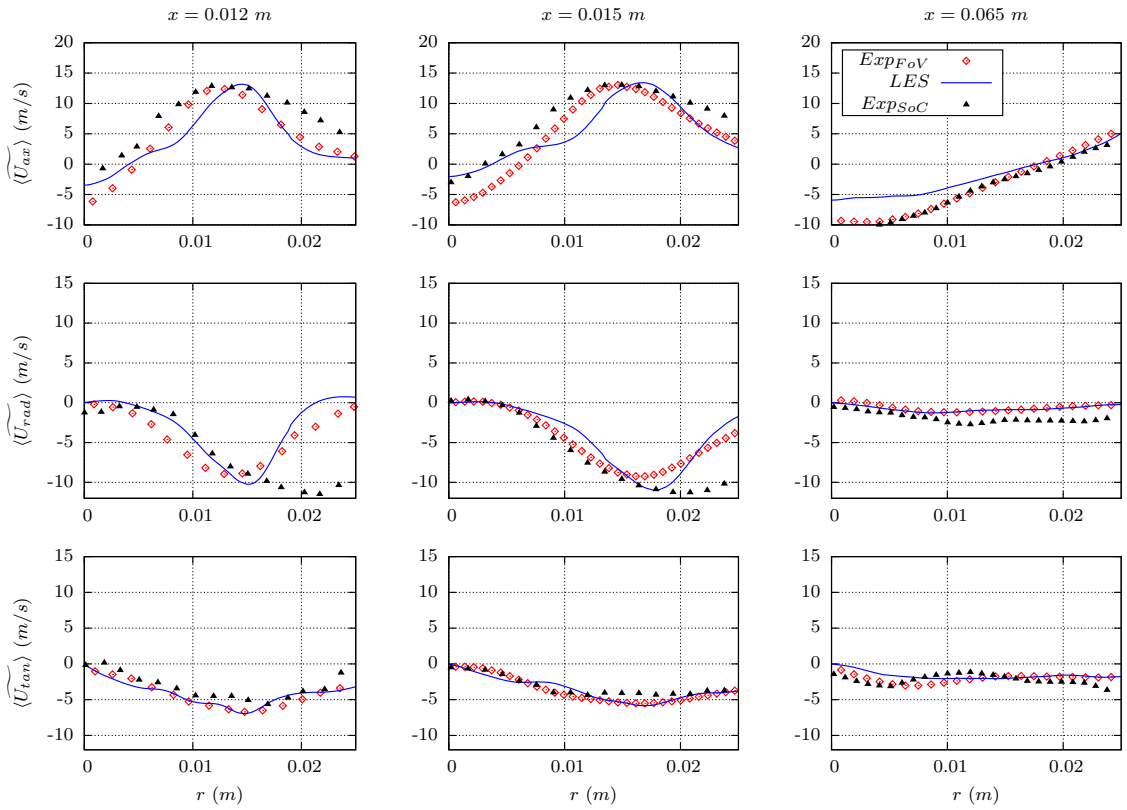

Fig. 3 Radial profiles of the mean axial, radial, and tangential velocity components at different axial positions compared with the experimental data from [17].

heat losses at the walls. More specifically, the temperature increase between x = 0 and 0.01 m is correctly captured, which indicates the correct location of the primary combustion zone. Then, the temperature increases to its maximum value at axial position x = 0.025 m, and decreases downstream due to the secondary air injection. It can be observed that the simulation captures the trend of measured temperature values but slightly under-predicts the temperature downstream of the secondary air injection. Measured and calculated temperatures at two different axial positions are compared in Fig. 6. Time-averaged values are given on the left and RMS values on the right side. At x = 0.018 m, hot gases are present at the centerline, while the heat losses through the walls lead to temperature decrease at higher radial positions. The secondary air injection at x = 0.080 m decreases the temperature on the centerline of the combustor. The agreement level of time-averaged values is satisfactory. Experimental RMS values indicate low level of turbulence at x = 0.080 m. In the LES, the temperature RMS at the centerline and in the near-wall region are well captured. Furthermore, the satisfactory agreement level of temperature fluctuations at higher radial positions suggests that the heat losses are well predicted. Overall a reasonably good agreement between simulated flow field and temperature and the experimental data is obtained.

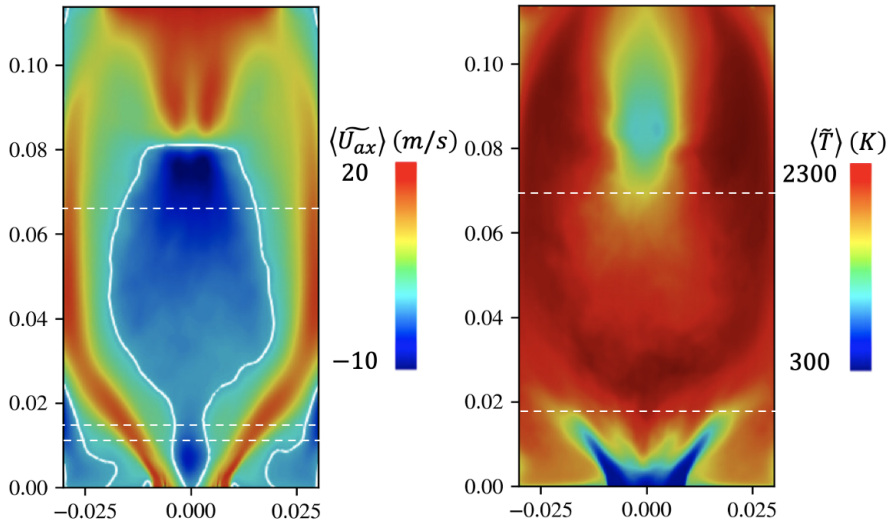

Fig. 4 Time-averaged axial velocity (left) and temperature (right) contours in a midplane of the combustor. The solid lines correspond to the zero axial velocity ($U_{ax} = 0$). Dashed lines correspond to selected axial positions for comparison with experimental data. Dimensions are in m.

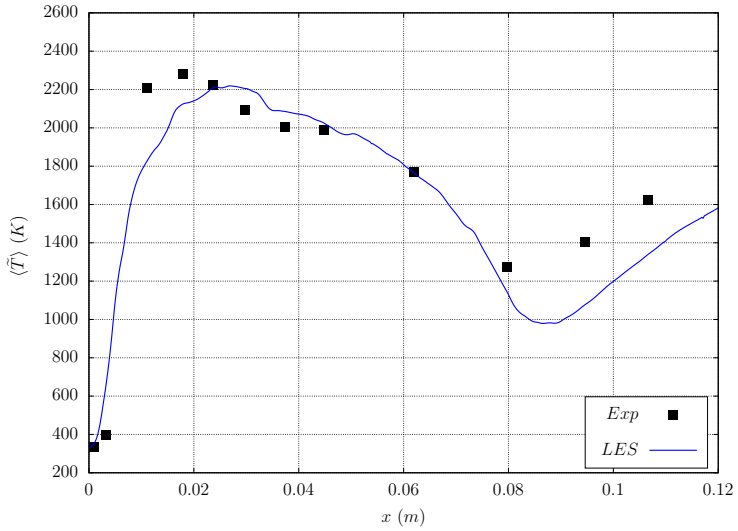

Fig. 5 Mean temperature along the centerline of the combustor compared with the experimental data from [18].

The time-averaged mixture fraction contour is illustrated in Fig. 7. The white line represents the stoichiometric mixture fraction isoline for $Z_{st} = 0.064$. Higher mixture fraction values are visible outside the inner recirculation zone. Further, the fuel-rich jet is deflected towards the wall, leading to richer mixture fraction values in the shear layers. The flow structure in Fig. 4 illustrates that the secondary oxidation air is not simply transported downstream but is predominantly entrained into the IRZ reducing the mixture fraction in the central part of the combustor.

To further investigate the dynamics of the flame and the related soot formation, instantaneous contours of the mixture fraction, acetylene mass fraction C_2H_2 and soot volume fraction in the combustor are shown in Fig. 8. It can be observed that a fuel-rich mixture, favorable to soot production, is formed only close to the swirler and close the combustor walls at downstream positions. The presence of secondary air is also indicated by the low mixture fraction values in the center of the combustor downstream of the position $x = 0.06$. In the fuel-rich mixture region, acetylene is formed in the proximity of the shear layers. The peak of the acetylene mass fraction is present in the primary combustion zone. It can be observed that peak values of the soot volume fraction are confined within the fuel-rich region close to the swirler

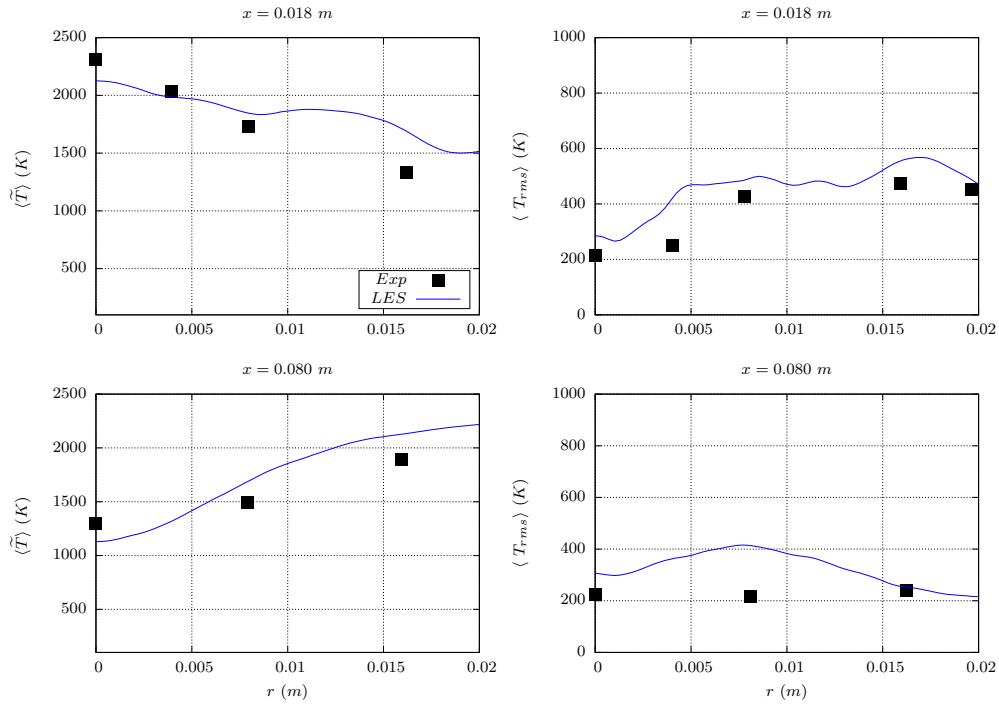

Fig. 6 Radial profiles of mean (left) and RMS (right) of the temperature at different axial positions compared with experimental data from [18].

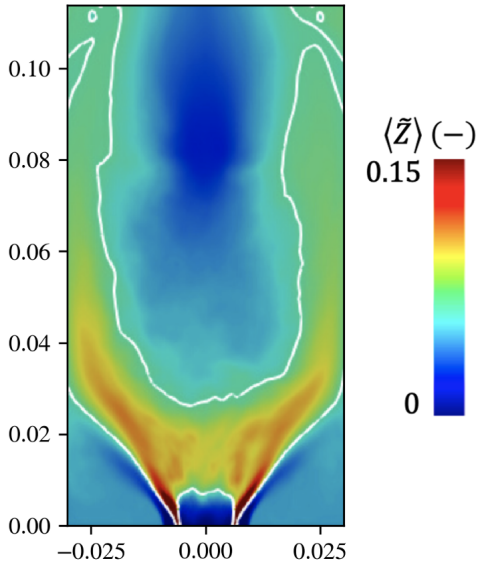

Fig. 7 Time-averaged mixture fraction contour in a midplane of the combustor. Solid lines show the stoichiometric mixture fraction (Z_{st} = 0.064). Dimensions are in m.

and in the areas of high acetylene mass fractions. The soot pockets are then transported downstream in the combustor close to the walls. Further, soot particles are not present in the area between the side jet stagnation region and the inner recirculation zone where a fuel-lean mixture is present.

A comparison of time-averaged and measured soot volume fraction is presented in Fig. 9. Computational results have been averaged over a physical time of about 30 ms. The S-EQMOM model predicts soot presence in the region

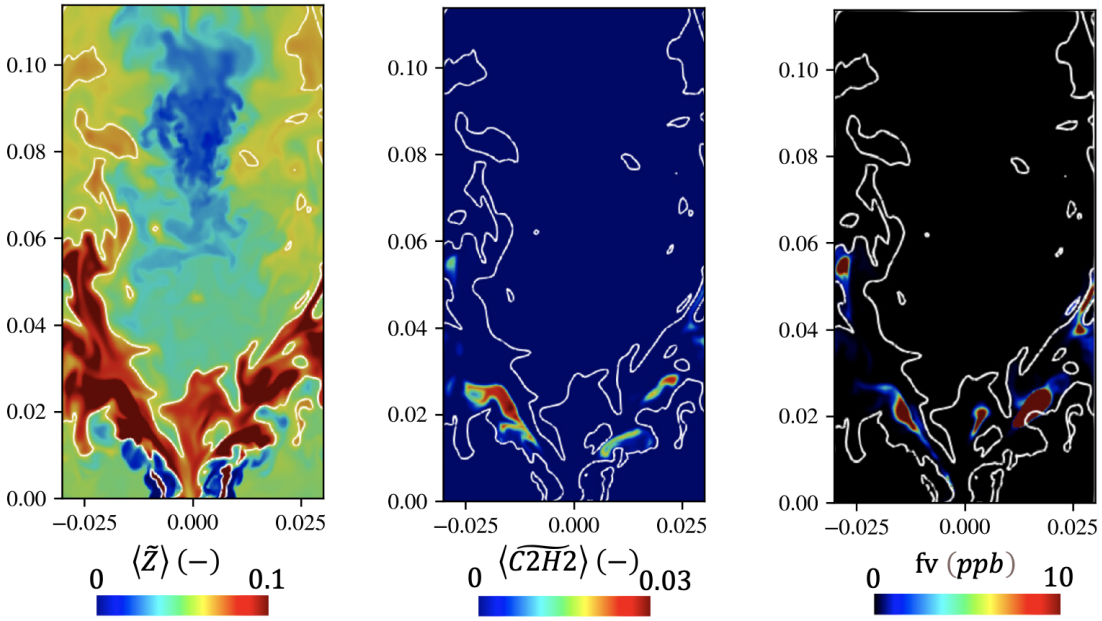

Fig. 8 Instantaneous contour of mixture fraction, PAH mass fraction and soot volume fraction on a centerplane of the combustor. Solid lines show the stoichiometric mixture fraction (Z_{st} = 0.064). Dimensions are in m.

between the flame front and the inner recirculation zone, similar to the measurements. Quantitatively, the soot volume fraction is under-predicted approximately by a factor of three. Further, experimental results indicate soot volume fraction in the center of the swirled flame stabilization zone, close to the primary swirler, which is not predicted by the simulation. This is consistent with previously published LES results with detailed soot models [8, 28, 43] and needs to be further investigated. Furthermore, soot is present close to walls of the combustion chamber. This behavior is captured in the simulations up to x = 0.06 m. Downstream this position, simulation results do not predict the presence of soot.

The simulation does not predict soot formation in the outer recirculation zone. Nevertheless, the measured soot presence in the ORZ seems to have resulted from an overlapping of the outer recirculation zone and soot formation in the shear layers [44]. Overall, a satisfactory qualitative agreement of soot volume fraction regarding its position and shape is obtained. Compared to the previous works on soot predictions of this configurations [8, 10, 28, 43], the results of the particulate phase show a good general agreement.

V. Conclusions

Large-Eddy Simulations of the DLR model aero-engine combustor have been performed for the 3 bar operating point with secondary air injection [20]. The recently developed Split-based Extended Method of Moments has been applied combined with a flamelet-progress variable tabulated chemistry approach and the ATF method. An additional transport equation for a lumped PAH species is considered to accurately account for the coupling between the gas and solid phase.

A good prediction of the velocity and temperature fields is obtained compared to the experimental data. The shape and the position of the inner recirculation zone are correctly captured by the LES.

The soot statistics predicted by the S-EQMOM are qualitatively in good agreement with the measurements. The time-averaged soot volume fraction is located within the fuel-rich regions and outside the inner recirculation zone, similar to the measurements. The soot volume fraction on the burner axis is not well predicted by the simulation, which requires further investigations. The quantitative comparison shows that soot is underestimated by a factor of three. Overall, the S-EQMOM model provided a satisfactory agreement with the experiments, yielding a continuous reconstruction of the particle NDF, which is crucial for an accurate prediction of the soot particle oxidation, as well as numerically robustness [14]. Future work will evaluate different soot nucleation models as well as the effect of gas and soot phase radiation on soot particle formation.

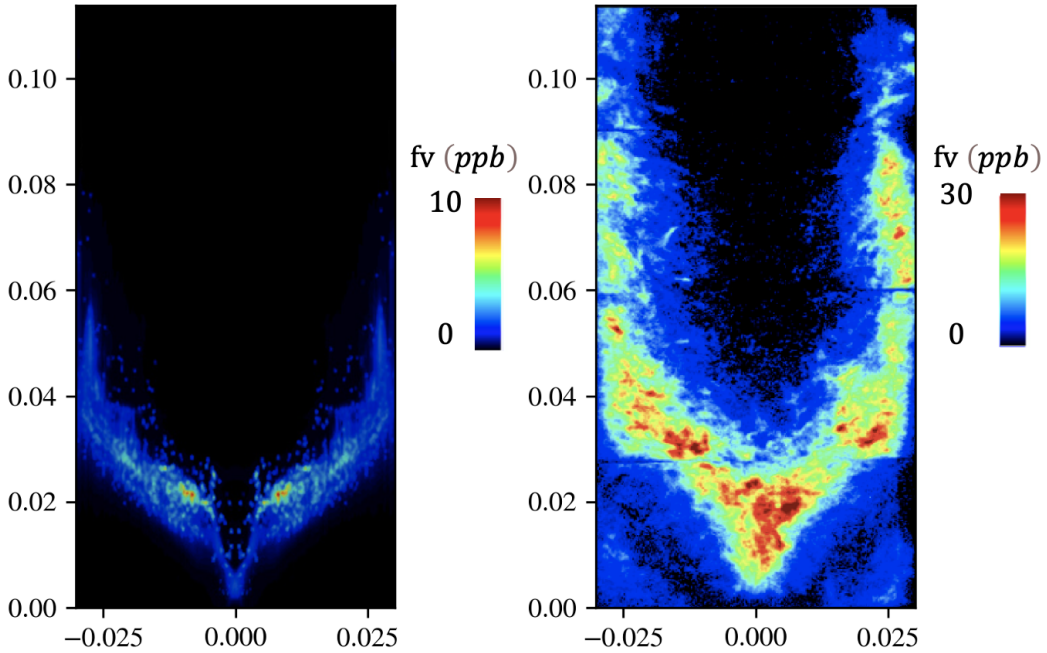

Fig. 9 Time-averaged soot volume fraction contour from LES (left) and experiments (right) [18]. Dimensions are in m.

Acknowledgements

This research has been funded by the Clean Sky 2 Joint Undertaking under the European Union's Horizon 2020 research and innovation programme under the ESTiMatE project, grant agreement No 821418. Calculations for this research were conducted on the Lichtenberg high-performance computer at TU Darmstadt.

References

[1] Rindlisbacher, T., and Jacob, S. D., "New Particulate Matter Standard for Aircraft Gas Turbine Engines," *ICAO Environmental Report*, 2011, pp. 85–88.

[2] Mueller, M. E., and Pitsch, H., "LES model for sooting turbulent nonpremixed flames," *Combust. Flame*, Vol. 159, No. 6, 2012, pp. 2166–2180.

[3] Han, W., Raman, V., Mueller, M. E., and Chen, Z., "Effects of combustion models on soot formation and evolution in turbulent nonpremixed flames," *Proc. Combust. Inst.*, Vol. 37, 2019, pp. 985–992.

[4] Sewerin, F., and Rigopoulos, S., "An LES-PBE-PDF approach for predicting the soot particle size distribution in turbulent flames," *Combust. Flame*, Vol. 189, 2018, pp. 62–76.

[5] Rodrigues, P., Franzelli, B., Vicquelin, R., Gicquel, O., and Darabiha, N., "Coupling an LES approach and a soot sectional model for the study of sooting turbulent non-premixed flames," *Combust. Flame*, Vol. 190, 2018, pp. 477–499.

[6] Ferraro, F., Gierth, S., Salenbauch, S., Han, W., and Hasse, C., "Large eddy simulation of the Delft Adelaide Flame III using a quadrature-based method of moments," *10th European Combustion Meeting*, 2021, pp. 913–918.

[7] Franzelli, B., Riber, E., Cuenot, B., and Ihme, M., "Numerical modeling of soot production in aero-engine combustors using large eddy simulations," *Proc. ASME Turbo Expo, GT2015-43630*, 2015.

[8] Eberle, C., Gerlinger, P., Geigle, K. P., and Aigner, M., "Numerical Investigation of Transient Soot Evolution Processes in an Aero-Engine Model Combustor," *Combust. Sci. Technol.*, Vol. 187, 2015, pp. 1841–1866.

[9] Chong, S. T., Hassanaly, M., Koo, H., Mueller, M. E., Raman, V., and Geigle, K. P., "Large eddy simulation of pressure and dilution-jet effects on soot formation in a model aircraft swirl combustor," *Combust. Flame*, Vol. 192, 2018, pp. 452–472.

[10] Wick, A., Priesack, F., and Pitsch, H., "Large-Eddy simulation and detailed modeling of soot evolution in a model aero engine combustor," *ASME Turbo Expo, GT2017-63293*, 2017.

[11] Grader, M., Eberle, C., Gerlinger, P., and Aigner, M., "LES of a pressurized, sooting aero-engine model combustor at different equivalence ratios with a sectional approach for pahs and soot," *Proceedings of the ASME Turbo Expo, GT2018-75254*, 2018.

[12] Rigopoulos, S., "Modelling of Soot Aerosol Dynamics in Turbulent Flow," *Flow, Turbul. Combust.*, Vol. 103, 2019, pp. 565–604.

[13] Yuan, C., Laurent, F., and Fox, R. O., "An extended quadrature method of moments for population balance equations," *J. Aerosol Sci.*, Vol. 51, 2012, pp. 1–23.

[14] Salenbauch, S., Hasse, C., Vanni, M., and Marchisio, D. L., "A numerically robust method of moments with number density function reconstruction and its application to soot formation, growth and oxidation," *J. Aerosol Sci.*, Vol. 128, 2019, pp. 34–49.

[15] Nguyen, T. T., Laurent, F., Fox, R. O., and Massot, M., "Solution of population balance equations in applications with fine particles: Mathematical modeling and numerical schemes," *J. Comput. Phys.*, Vol. 325, 2016, pp. 129–156.

[16] Pigou, M., Morchain, J., Fede, P., Penet, M. I., and Laronze, G., "New developments of the Extended Quadrature Method of Moments to solve Population Balance Equations," *J. Comput. Phys.*, Vol. 365, 2018, pp. 243–268.

[17] Geigle, K. P., Hadef, R., Stöhr, M., and Meier, W., "Flow field characterization of pressurized sooting swirl flames and relation to soot distributions," *Proc. Combust. Inst.*, Vol. 36, 2017, pp. 3917–3924.

[18] Geigle, K. P., Köhler, M., O'Loughlin, W., and Meier, W., "Investigation of soot formation in pressurized swirl flames by laser measurements of temperature, flame structures and soot concentrations," *Proc. Combust. Inst.*, Vol. 35, 2015, pp. 3373–3380.

[19] Geigle, K. P., O'Loughlin, W., Hadef, R., and Meier, W., "Visualization of soot inception in turbulent pressurized flames by simultaneous measurement of laser-induced fluorescence of polycyclic aromatic hydrocarbons and laser-induced incandescence, and correlation to OH distributions," *Appl. Phys. B*, Vol. 119, 2015, pp. 717–730.

[20] Geigle, K. P., Hadef, R., and Meier, W., "Soot Formation and flame characterization of an aero-engine model combustor burning ethylene at elevated pressure," *J. Eng. Gas Turbines Power*, Vol. 136, 2014, pp. 1–7.

[21] Dupoirieux, F., and Bertier, N., "Methodology for the numerical prediction of soot formation in turbulent reactive flows and application to aircraft engine combustors," *IJSA*, Vol. 2, 2016, p. 15.

[22] Felden, A., Riber, E., and Cuenot, B., "Impact of direct integration of Analytically Reduced Chemistry in LES of a sooting swirled non-premixed combustor," *Combust. Flame*, Vol. 191, 2018, pp. 270–286.

[23] Chong, S. T., Raman, V., Mueller, M. E., Selvaraj, P., and Im, H. G., "Effect of soot model, moment method, and chemical kinetics on soot formation in a model aircraft combustor," *Proc. Combust. Inst.*, Vol. 37, 2019, pp. 1065–1074.

[24] Leung, K. M., Lindstedt, R. P., and Jones, W. P., "A simplified reaction mechanism for soot formation in nonpremixed flames," *Combust. Flame*, Vol. 87, No. 3-4, 1991, pp. 289–305.

[25] Mueller, M. E., Blanquart, G., and Pitsch, H., "Hybrid Method of Moments for modeling soot formation and growth," *Combust. Flame*, Vol. 156, 2009, pp. 1143–1155.

[26] Yuan, C., and Fox, R. O., "Conditional quadrature method of moments for kinetic equations," *J. Comput. Phys.*, Vol. 230, No. 22, 2011, pp. 8216–8246.

[27] Gallen, L., Felden, A., Riber, E., and Cuenot, B., "Lagrangian tracking of soot particles in les of gas turbines," *Proc. Combust. Inst.*, Vol. 37, No. 4, 2019, pp. 5429–5436.

[28] Rodrigues, P., "Modélisation multiphysique de flammes turbulentes suitées avec la prise en compte des transferts radiatifs et des transferts de chaleur pariétaux," Ph.D. thesis, Université Paris-Saclay Français, 2018.

[29] Nau, P., Yin, Z., Geigle, K. P., and Meier, W., "Wall temperature measurements at elevated pressures and high temperatures in sooting flames in a gas turbine model combustor," *Appl. Phys. B*, Vol. 123, 2017, pp. 1–8.

[30] Tardelli, L. P., Darabiha, N., Veynante, D., and Franzelli, B., "Contribution of Soot Subgrid Intermittency Model To the Prediction of Soot Production in an Aero-Engine Model Combustor," *Proceedings of the ASME Turbo Expo, GT2019-90873*, 2021.

[31] Nicoud, F., Toda, H. B., Cabrit, O., Bose, S., and Lee, J., "Using singular values to build a subgrid-scale model for large eddy simulations," *Phys. Fluids*, Vol. 23, 2011.

[32] Pierce, C. D., and Moin, P., "Progress-variable approach for large-eddy simulation of non-premixed turbulent combustion," *J. Fluid Mech.*, Vol. 504, 2004, pp. 73–97.

[33] Ihme, M., Cha, C. M., and Pitsch, H., "Prediction of local extinction and re-ignition effects in non-premixed turbulent combustion using a flamelet/progress variable approach," *Proc. Combust. Inst.*, Vol. 30, No. 1, 2005, pp. 793–800.

[34] Zschutschke, Axel; Messig, Danny; Scholtissek, Arne; Hasse, C., "Universal Laminar Flame Solver (ULF)," *https://figshare.com/articles/poster/ULF-code-pdf/5119855*, 2017.

[35] Steinhausen, M., Luo, Y., Popp, S., Strassacker, C., Zirwes, T., Kosaka, H., Zentgraf, F., Maas, U., Sadiki, A., Dreizler, A., and Hasse, C., "Numerical Investigation of Local Heat-Release Rates and Thermo-Chemical States in Side-Wall Quenching of Laminar Methane and Dimethyl Ether Flames," *Flow Turbul. Combust.*, 2021, pp. 681–700.

[36] Popp, S., Hartl, S., Butz, D., Geyer, D., Dreizler, A., Vervisch, L., and Hasse, C., "Assessing multi-regime combustion in a novel burner configuration with large eddy simulations using tabulated chemistry," *Proc. Combust. Inst.*, Vol. 38, 2020, pp. 2551–2558.

[37] Blanquart, G., "Effects of spin contamination on estimating bond dissociation energies of polycyclic aromatic hydrocarbons," *Int. J. Quantum Chem.*, Vol. 115, 2015, pp. 796–801.

[38] Narayanaswamy, K., Blanquart, G., and Pitsch, H., "A consistent chemical mechanism for oxidation of substituted aromatic species," *Combust. Flame*, Vol. 157, 2010, pp. 1879–1898.

[39] Colin, O., Ducros, F., Veynante, D., and Poinsot, T., "A thickened flame model for large eddy simulations of turbulent premixed combustion," *Phys. Fluids*, Vol. 1843-1863, 2000.

[40] Charlette, F., Meneveau, C., and Veynante, D., "A power-law flame wrinkling model for LES of premixed turbulent combustion Part I: Non-dynamic formulation and initial tests," *Combust. Flame*, Vol. 131, 2002, pp. 159–180.

[41] Popp, S., Kuenne, G., Janicka, J., and Hasse, C., "An extended artificial thickening approach for strained premixed flames," *Combust. Flame*, Vol. 206, 2019, pp. 252–265.

[42] Popp, S., Hunger, F., Hartl, S., Messig, D., Coriton, B., Frank, J. H., Fuest, F., and Hasse, C., "{LES} flamelet-progress variable modeling and measurements of a turbulent partially-premixed dimethyl ether jet flame," *Combust. Flame*, Vol. 162, 2015, pp. 3016–3029.

[43] Koo, H., Raman, V., Mueller, M. E., and Geigle, K. P., "LES of a sooting flame in a pressurized swirl combustor," *54th AIAA Aerospace Sciences Meeting*, 2016, pp. 1–13.

[44] Eberle, C., Gerlinger, P., Geigle, K. P., and Aigner, M., "Toward finite-rate chemistry large-eddy simulations of sooting swirl flames," *Combust. Sci. Technol.*, Vol. 190, 2018, pp. 1194–1217.